Structural Characteristics and Redox Behaviors of $Ce_{1-x}Cu_xO_y$ Solid Solutions

Wenjuan Shan, Wenjie Shen,* and Can Li*

State Key Laboratory of Catalysis, Dalian Institute of Chemical Physics, Chinese Academy of Sciences, Dalian 116023, China

Received July 8, 2003. Revised Manuscript Received September 22, 2003

Nanosized $Ce_{1-x}Cu_xO_y$ materials were prepared by complexation−combustion method. The structural characteristics and redox behaviors were investigated using X-ray diffraction (XRD), temperature programmed reduction (H_2-TPR), UV−Vis, and Raman spectroscopies. In XRD patterns, no evidence of CuO diffraction peaks are observed for the $Ce_{1-x}Cu_xO_y$ samples calcinated at 650 °C for 5 h, until the Cu/(Ce + Cu) ratio is higher than 0.4. The stepwise decrease of the 2θ value of CeO_2 in $Ce_{1-x}Cu_xO_y$ with the increasing of Cu concentration suggests that the Cu^{2+} ions incorporate into the CeO_2 lattice to form $Ce_{1-x}Cu_xO_y$ solid solutions for low Cu/(Ce + Cu) ratios ($x \leq 0.1$). The CuO phase begins to segregate from the solid solutions with the further increasing of Cu/(Ce+Cu) ratio. The Raman mode at 1176 cm^{-1} ascribed to the enhanced defects appears for CeO_2 and the $Ce_{0.9}Cu_{0.1}O_y$ solid solution. Compared with CeO_2 alone, the Raman mode of cubic CeO_2 shifts from 462 to 443 cm^{-1} for the $Ce_{0.9}Cu_{0.1}O_y$ solid solution. The H_2 consumption of the fresh $Ce_{0.95}Cu_{0.05}O_y$ is 1.65 times higher than that needed to reduce CuO to Cu, and it increases to 2.4 after a reoxidation of the partially reduced $Ce_{0.95}Cu_{0.05}O_y$ at 300 °C, which indicates that the CeO_2 phase is also extensively reduced. Compared with the high Cu/(Ce+Cu) ratio sample $Ce_{0.7}Cu_{0.3}O_y$, the $Ce_{0.9}Cu_{0.1}O_y$ solid solution shows high and stable redox property even after different reoxidation temperatures. When the reoxidation temperature exceeds 200 °C, the α peak (∼170 °C) ascribed to the reduction of surface oxygen disappears, and the β peak (∼190 °C) ascribed to the reduction of Cu^{2+} species and the partial reduction of bulk CeO_2 shifts to higher temperatures with the H_2 consumption 1.16 times higher than that for fresh sample. The result demonstrates that the redox property of the CeO_2 is significantly improved by forming the $Ce_{1-x}Cu_xO_y$ solid solutions.

Introduction

Recently, CeO_2 and CeO_2-based materials have attracted much attention in catalysis because of their unique catalytic activities in reactions associated with environmental concerns.[1−3] The facile Ce^{4+}/Ce^{3+} redox cycle often leads to higher oxygen storage capacity (OSC) with reversible addition and removal of oxygen in the fluorite structure of ceria. For further improvement of the redox cycle between Ce^{4+} and Ce^{3+}, various CeO_2-based binary oxides, such as $CeO_2-Al_2O_3$,[4] $CeO_2-La_2O_3$,[5] CeO_2-HfO_2,[6] $CeO_2-Sm_2O_3$,[3] CeO_2-TiO_2,[7] and CeO_2-ZrO_2,[8,9] have been widely investigated. A general conclusion is that the incorporation of MO_x into the CeO_2 lattice forms $Ce_{1-x}M_xO_y$ solid solutions with higher OSC and better redox properties than those of CeO_2 alone.

However, only a few investigations have been reported[10−13] on the preparation, property, and application of transitional metals or noble metals-doped CeO_2 solid solutions, although some studies of CeO_2-based solid solutions were focused on as materials for solid oxide fuel cells, oxygen sensors, and catalyst supporters.[1,14] As a matter of fact, ceria-containing materials have been applied in various catalytic reactions owing to the unique SMSI (strong metal−support interaction) between the surface oxygen vacancies and the metal oxide species and its effects on redox property and on

* Authors to whom correspondence should be addressed. Fax: 86-411-4694447. E-mail: shen98@dicp.ac.cn; canli@dicp.ac.cn.

(1) He, H.; Dai, H. X.; Ng, L. H.; Wong, K. W.; Au, C. T. *J. Catal.* **2002**, *206*, 1.
(2) Liu, Y.; Hayakawa, T.; Suzuki, K.; Hamakawa, S.; Tsunoda, T.; Ishii, T.; Kumagai, M. *Appl. Catal., A* **2002**, *223*, 137.
(3) Li, L.; Li, G.; Che, Y.; Su, W. *Chem. Mater.* **2000**, *12*, 2567.
(4) Bensalem, A.; Bozon Verduraz, F.; Delamar, M.; Bugli, G. *Appl. Catal.* **1995**, *121*, 81.
(5) Usman, R. K.; Graham, G. W.; Watkins, W. L. H.; McCabe, R. W. *Catal. Lett.* **1995**, *30*, 53.
(6) Zamar, F.; Trovarelli, A.; De Leitenburg, C.; Dolcetti, G. *J. Chem. Soc. Chem. Commun.* **1995**, 965.
(7) Luo, M.; Chen, J.; Lu, J.; Feng, Z.; Li, C. *Chem. Mater.* **2001**, *13*, 1491.
(8) Kozlov, A. I.; Kim, D. H.; Yezerets, A.; Andersen, P.; Kung, H. H.; Kung, M. C. *J. Catal.* **2002**, *209*, 417.
(9) Sergent, N.; Lamonier, J.; Aboukaïs, A. *Chem. Mater.* **2000**, *12*, 3830.
(10) Bera, P.; Priolkar, K. R.; Sarode, P. R.; Hegde, M. S.; Emura, S.; Kumashiro, R.; Lalla, N. P. *Chem. Mater.* **2002**, *14*, 3591.
(11) Priolkar, K. R.; Bera, P.; Sarode, P. R.; Hegde, M. S.; Emura, S.; Kumashiro, R.; Lalla, N. P. *Chem. Mater.* **2003**, *14*, 2120.
(12) Bera, P.; Priolkar, K. R.; Gayen, A.; Sarode, P. R.; Hegde, M. S.; Emura, S.; Kumashiro, R.; Jsysrsm, V.; Subbanna, G. N. *Chem. Mater.* **2003**, *15*, 2049.
(13) Nagaveni, K.; Sivalingam, G.; Gayen, A.; Madras, G.; Hegde, M. S. *Catal. Lett.* **2003**, *88* (1−2), 73.
(14) Li, J.; Ikegami, T.; Mori, T.; Wada, T. *Chem, Mater.* **2001**, *13*, 2913.

10.1021/cm0345974 CCC: $25.00
Published on Web 10/28/2003

catalytic activities.[15] For example, CuO/CeO_2 catalysts were reported to exhibit high catalytic activities toward NO reduction and oxidations of CO and hydrocarbons.[16−23] A synergistic reaction pathway was proposed to explain the enhanced catalytic activity in CO oxidation,[24−26] in which both the CeO_2 and the copper oxides are simultaneously reduced or oxidized with CO or O_2 respectively. It turned out that the electronic interaction between CuO and CeO_2 plays an important role in enhancing the catalytic activity. This fact was further confirmed by cyclic voltammetry investigations and temperature-programmed reaction studies.[27]

The enhanced redox property of CeO_2 could be obtained by incorporating a transitional metal to the cubic CeO_2 lattice to form solid solution.[28] However, it is still difficult to obtain the $Ce_{1-x}Cu_xO_y$ solid solutions using traditional preparation methods such as impregnation, coprecipitation, and decomposition−precipitation. In the present study, nanosized $Ce_{1-x}Cu_xO_y$ ($x \leq 0.1$) solid solutions are prepared by the complexation−combustion method. The structural evidence of the solid solutions with the enhanced oxygen vacancies was provided by XRD, UV−vis, and Raman spectra studies. The H_2-TPR experiment further indicates that the reduction of CeO_2 is not limited to the surface oxygen but extends to the bulk oxygen in the reduction−oxidation processes, which is the reason for the enhanced redox property in the solid solutions.

Experimental Section

Sample Preparation. The $Ce_{1-x}Cu_xO_y$ materials were prepared by citric acid complexation−combustion method. $Ce(NO_3)_3 \cdot 6H_2O$ and $Cu(NO_3)_2 \cdot 3H_2O$ were dissolved in deionized water in such a manner to give solution of 1.0 M. Citric acid was added with 1.2× molar amounts to the premixed nitrate solutions of cerium and copper with different Cu/Ce ratios. The solution temperature was kept at 70 °C for 2 h. In the process, the mixture color changed from blue to green and the pH value was about 1.0. Once the gel formed, the temperature was elevated to 150 °C quickly, the gel foamed, with production of nitrogen oxide vapors, and burnt with sparks. A solid product was obtained after the sparks were extinguished. For this process, it is suggested to select open containers (such as a Bunsen beaker), and it is safe to operate in a ventilated environment. The resulting powder calcined at 650 °C for 5 h in air is referred to as fresh sample. The notation of *x*, *y* in the samples means the atomic ratio. The reference Ce/Cu sample is a physical mixture of CeO_2 and CuO with an atom ratio of 1:1.

Table 1. BET Surface Areas and Pore Parameters of $Ce_{1-x}Cu_xO_y$

sample	BET (m^2/g)	pore volume (cc/g) × 10^{-2}	pore diameter (Å)
$x = 0.05$	34.5	8.8	102.0
$x = 0.1$	29.8	8.8	118.5
$x = 0.3$	17.5	5.3	120.3
$x = 0.5$	16.8	4.6	108.3

Catalyst Characterization. The specific surface areas of the samples were obtained at 77 K using a Micromeritics ASAP 2010. The BET area and the pore size were calculated by using the adsorption and desorption branches, respectively. Prior to measuring, the samples were pretreated in vacuo at 300 °C for 2 h.

X-ray powder diffraction (XRD) patterns were recorded on a Rigaku Rotaflex (RU-200B) powder diffractometer using nickel-filtered Cu Kα radiation. The mean crystallite size of cubic phase was calculated from the Scherrer equation, where the Scherrer constant (particle shape factor) was taken as 0.89. The lattice parameters were calculated according to the Cohen procedure.[29]

UV−Visible diffuse reflectance spectra were recorded on a JASCO V-550 UV−Visible spectrophotometer.

UV Raman spectra were recorded on a homemade UV Raman spectrograph which had four key parts: a UV cw laser, a Spex 1877d triplemate spectrograph, a CCD detector, and an optical collection system. A line at 325 nm from a He−Cd laser with an output of 25 mW is used for excitation source of the UV Raman spectroscopy. The laser power measured at the samples was below 4.0 mW for 325 nm radiation.

Visible Raman spectra were recorded on a Jobin-Yvon U1000 scanner with a 532-nm single-frequency laser. Samples were mounted in a spinning holder to avoid thermal damage during the spectrum scanning, which usually takes about 5 min. The Raman signal was collected with a 90° geometry. The spectra of all samples were recorded at room temperature.

Temperature-programmed reduction (TPR) was conducted using a conventional apparatus equipped with a TCD detector. A molecular sieve trap was placed before the detector to adsorb the produced water. TPR was performed by heating the sample (50 mg) at 10 °C/min to 500 °C in a 5% H_2-N_2 mixture flowing at 40 mL/min. Then, the reduced samples were reoxidized at 300 °C for 2 h with 20% O_2/N_2. Repeated temperature-programmed reduction measurements were performed following the reoxidation after cooling the sample in pure N_2.

Results and Discussion

Structural Characteristics of $Ce_{1-x}Cu_xO_y$ Materials. Table 1 gives the surface areas and pore structure parameters of the samples being calcinated at 650 °C. It can be seen that the BET area decreased with the increase of the Cu/Ce + Cu ratio in the samples. With the increasing of the Cu molar ratio from 0.05 to 0.3, the specific surface area of the samples decreased from 34.5 to about 17.5 m^2/g, whereas further increasing the ratio of Cu from 0.3 to 0.5 did not cause any decrease in surface area. The dependence of the pore volume on the content of Cu in the samples is consistent with that of the BET area. However, the N_2 adsorption and desorption experiments showed that the pore size is not uniform — in the range from 10 to 12 nm for all the samples.

(15) Matsumura, Y.; Shen, W. J.; Ichihashi, Y.; Ando, H. *Catal. Lett.* **2000**, *68*, 181.
(16) Liu, W.; Flytzani-Stephanopoulos, M. *J. Catal.* **1995**, *153*, 304.
(17) Hu, Y.; Dong, L.; Wang, J.; Ding, W.; Chen, Y. *J. Mol. Catal. A: Chem.* **2000**, *162*, 307.
(18) Kundakovic, Lj.; Flytzani-Stephanopoulos, M. *J. Catal.* **1998**, *179*, 203.
(19) Bera, P.; Aruna, S. T.; Patil, K. C.; Hegde, M. S. *J. Catal.* **1999**, *186*, 36.
(20) Skårman, B.; Grandjean, D.; Benfield, R. E.; Hinz, A.; Andersson, A.; Wallenberg, L. R. *J. Catal.* **2002**, *211*, 119.
(21) Martínez-Arias, A.; Soria, J.; Conesa, J. C.; Seoane, X. L.; Arcoya, A.; Cataluña, R. *J. Chem. Soc., Faraday Trans.* **1995**, *91*, 1679.
(22) Sedmak, G.; Hočevar, S.; Levec, J. *J. Catal.* **2003**, *213*, 135.
(23) Kim, D. H.; Cha, J. E. *Catal. Lett.* **2003**, *86* (1−3), 107.
(24) Martínez-Arias, A.; Soria, J.; Cataluña, R.; Conesa, J. C.; Cortés Corberán, V. *Stud. Surf. Sci. Catal.* **1998**, *116*, 591.
(25) Martínez-Arias, A.; Fernández-García, M.; Soria, J.; Conesa, J. C. *J. Catal.* **1999**, *182*, 367.
(26) Martínez-Arias, A.; Fernández-García, M.; Gálvez, O.; Coronado, J. M.; Anderson, J. A.; Conesa, J. C.; Soria, J.; Munuera, G. *J. Catal.* **2000**, *195*, 207.
(27) Bera, P.; Mitra, S.; Sampath, S.; Hegde, M. S. *Chem. Commun.* **2001**, 927.
(28) Machida, M.; Uto, M.; Kurogi, D.; Kijima, T. *Chem. Mater.* **2000**, *12*, 3158.
(29) Klug, H. P.; Alexander, L. E. *X-ray Diffraction Procedures*; John Wiley: New York, 1954.

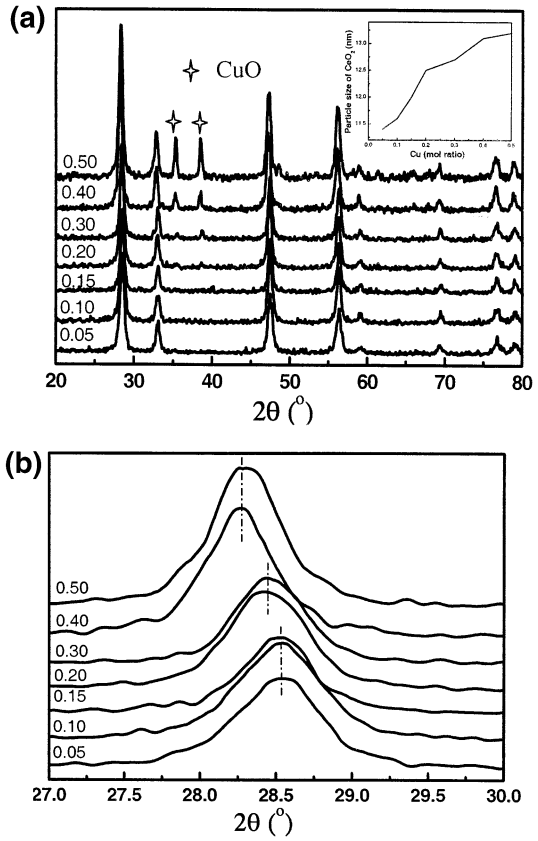

Figure 1. XRD patterns of $Ce_{1-x}Cu_xO_y$ (x = 0.05, 0.1, 0.15, 0.2, 0.3, 0.4, 0.5) calcinated at 650 °C.

Figure 1(a) shows the XRD patterns of $Ce_{1-x}Cu_xO_y$ samples with different copper ratios. It can be seen that no CuO phases can be identified for Cu/(Ce + Cu) ratios lower than 0.15, and very weak CuO reflections are observed with x ranging from 0.2 to 0.3, whereas apparent CuO diffraction peaks appear when $x \geq 0.4$. Meanwhile, the corresponding particle size of CeO_2 was found to increase with increasing Cu molar ratios. The CuO diffraction peaks previously observed to appear in a $Ce_{0.85}Cu_{0.15}O_y$ prepared by magnetron sputtering method and calcinated at 500 °C, further apparent intensity was observed when it was calcinated at 650 °C.[30] In the present study, the CuO diffraction peaks become distinct only when the Cu/(Ce + Cu) ratio is higher than 0.4. The usual explanation is that either the CuO is amorphic or it is well dispersed on the surface of ceria in the form of small clusters that cannot be detected by XRD.[26] Taking the calcination temperature and the BET surface area into account, the temperature at 650 °C is enough for the formation of CuO crystalloid, and the surface area about 17.5 m^2/g is too small to well disperse the CuO on the surface of CeO_2 for the $Ce_{0.7}Cu_{0.3}O_y$ sample. Therefore, it is highly possible that CuO is incorporated into the CeO_2 lattice at low Cu/(Ce + Cu) ratios instead of being strongly bounded and well dispersed on the surface of ceria in the form of small clusters.

The decrease in lattice parameters of ceria in the $Ce_{1-x}Cu_xO_y$ samples also provided evidence that some

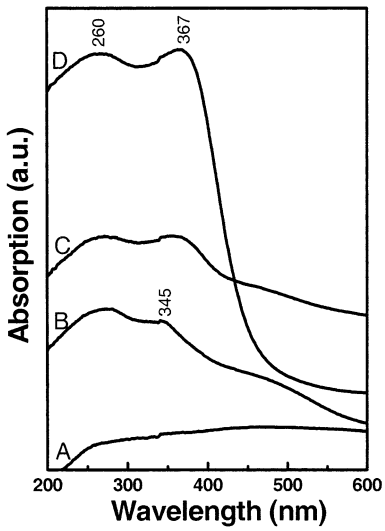

Figure 2. UV−Vis results for A, CuO; B, $Ce_{0.9}Cu_{0.1}O_y$; C, CeO_2/CuO = 1:1; D, CeO_2.

Cu^{2+} ions are incorporated into ceria lattice to form the $Ce_{1-x}Cu_xO_y$ solid solutions by considering the radius of Cu^{2+} ions (0.072 nm) is smaller than that of Ce^{4+} ions (0.101 nm). As shown in Figure 1(b), the position of CeO_2 diffraction peaks gradually shifted to low 2θ values with increasing the Cu level from 0.05 to 0.3. The further reduced 2θ values of CeO_2 diffraction peaks were observed when $x \geq 0.4$. The stepwise decrease of 2θ values with the increase of Cu/(Ce + Cu) ratio also indicated that the distribution of Cu species depends on the Cu/(Ce + Cu) ratio. Most Cu^{2+} ions incorporate into CeO_2 to form solid solutions at $x \leq 0.15$, and the Cu^{2+} ions segregate gradually from $Ce_{1-x}Cu_xO_y$ solid solutions with further increase of Cu content. The $Ce_{1-x}Cu_xO_y$ solid solutions and small CuO clusters coexist in the x range from 0.15 to 0.3, and the Cu^{2+} ions are mainly in the form of bulk CuO at higher Cu/(Ce + Cu) ratios.

Figure 2 shows the UV−Vis spectroscopies of CeO_2, CuO, Ce/Cu, and $Ce_{0.9}Cu_{0.1}O_y$ samples. A featureless spectrum is obtained for pure CuO. Two broad bands at 260 and 367 nm, respectively, in a physical mixture of CeO_2 and CuO are attributed to CeO_2, no contribution from CuO can be observed. In the $Ce_{0.9}Cu_{0.1}O_y$ solid solution, the constant band at 260 nm can be ascribed to the intrinsic character of CeO_2 accordingly, while the adsorption edge at 367 nm is blue-shifted and weakened. This blue shift may indicate the formation of CeO_2−CuO solid solution, which results in the increasing of splitting between appropriate electron levels and, as a consequence, increasing energy of transition. So it can be concluded that the 367-nm band is related to the defect structure of CeO_2. The shift and the reduced intensity of the 367-nm band might be ascribed to the enhanced defect structure due to the formation of $Ce_{0.9}Cu_{0.1}O_y$ solid solution.

Figure 3 shows the UV−Raman spectra recorded by using a laser at 325 nm as the excitation source. A broad band with relatively high intensity was observed at 462 cm^{-1} for cubic CeO_2 in the $Ce_{0.9}Cu_{0.1}O_y$ solid solution together with two bands at about 584 and 1176 cm^{-1}. Compared with CeO_2, the physical mixture (CeO_2/CuO = 1:1) sample showed the reduced Raman modes due

(30) Tschöpe A.; Trudeau M. L.; Ying J. Y. *J. Phys. Chem. B* **1999**, *103*, 8858.

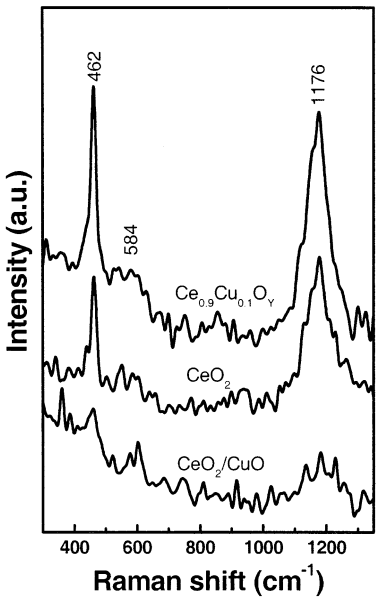

Figure 3. Raman spectra of samples excitated by 325-nm laser line.

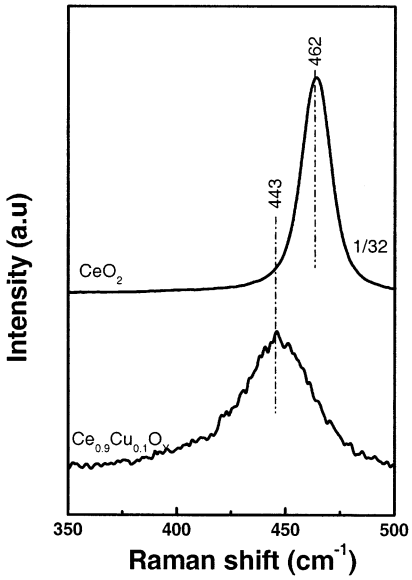

Figure 4. Raman spectra of samples excitated by 532-nm laser line.

to the strong adsorption of CuO in the region; whereas the enhanced Raman modes were observed in the $Ce_{0.9}Cu_{0.1}O_y$ solid solution that increased the defects by creating more oxygen vacancies. This fact also provides direct evidence that the Cu^{2+} ions incorporate in the CeO_2 lattice, instead of dispersing on the surface of CeO_2. But the Cu^{2+} ions in the CeO_2 lattice do not change the cubic structure of CeO_2, which is confirmed by the present of the band at 462 cm^{-1}. Therefore, the bands at 584 and 1176 cm^{-1} can be assigned to the defects of ceria fluorite structure. A weak peak between 550 and 600 cm^{-1} and a weaker second-order peak at about 1184 cm^{-1} (relative to the 462 cm^{-1}), which were attributed to the presence of CeO_2 defects, were reported in the literature when using a laser at 488 nm as the excitation source.[31] However, in the present study, a weak peak at 584 cm^{-1} and a peak at 1176 cm^{-1} with intensity similar to that of the peak at 462 cm^{-1} were observed. The increasing peak intensity at 1176 cm^{-1} might be due to the resonance Raman enhancement.

Figure 4 further compares the visible Raman spectra between the pure CeO_2 and the $Ce_{0.9}Cu_{0.1}O_y$ solid solution. A sharp peak at 462 cm^{-1} ascribed to cubic CeO_2 was observed, whereas the peak shifted from 462 to 443 cm^{-1} and became broad in the $Ce_{0.9}Cu_{0.1}O_y$ solid solution. This shift may imply that changes in the lattice parameter with particle size have occurred, as it was previously reported that a change of the particle size of CeO_2 from 6 nm to 5 μm leads to a shifted peak position about 10 cm^{-1}.[31] Another reason of shifting and broadening may be the presence of oxygen vacancies, corresponding to stoichiometry $CeO_{2-\delta}$, which is related to a change of CeO_2 environment in the presence of copper due to the formation of solid solution.

Redox Property of $Ce_{1-x}Cu_xO_y$ Materials. The TPR profiles of $Ce_{1-x}Cu_xO_y$ samples are shown in Figure 5. The hydrogen consumption can be roughly divided into two parts with the maximum reduction temperatures, which are named α and β, respectively. The intensity of α peak initially increased with increasing Cu/(Ce + Cu) ratio for solid solutions ($x \leq 0.1$), then it reduced gradually with the further increase of Cu ratio. The phenomena demonstrate that the α peak is related to the formation of solid solutions. As for the β peak, it is more complex. The reduction temperature was higher, as well as the peak with shoulders was broader and the intensity increased with an increasing Cu/(Ce + Cu) ratio. For example, the reduction temperature shifted from 190 to 310 °C when x increased from 0.05 to 0.5. It is named as γ peak for the samples $x \geq 0.2$. These TPR profiles also indicated that the distribution of Cu^{2+} species strongly depends on the Cu content in the $Ce_{1-x}Cu_xO_y$ materials as described in XRD results. For lower Cu/(Ce + Cu) ratio samples ($x < 0.2$), the reduction temperature of Cu^{2+} species in the solid solutions is reduced, the β peak is mainly contributed to its reduction. With increasing x, the reduction behavior of

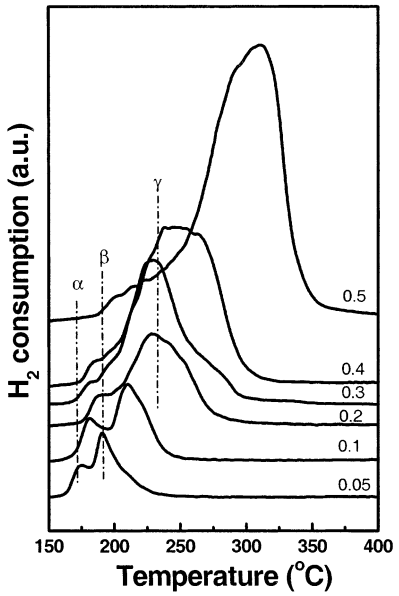

Figure 5. TPR profiles of $Ce_{1-x}Cu_xO_y$ ($x = 0.05$, 0.1, 0.2, 0.3, 0.4, 0.5).

(31) Spanier, J. E.; Robinson, R. D.; Zhang, F.; Chan, S. W.; Herman, I. P. *Phys. Rev. B* **2001**, *64*, 245407.

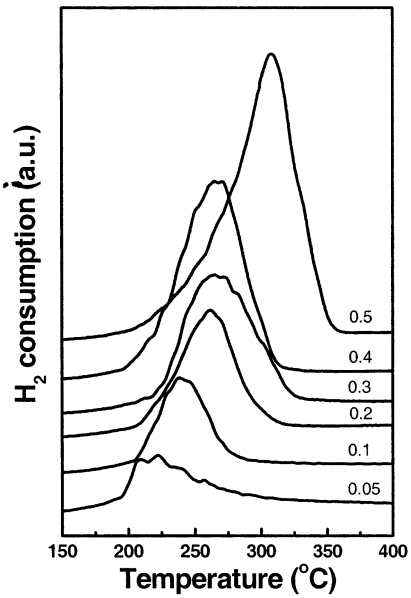

Figure 6. TPR profiles of $Ce_{1-x}Cu_xO_y$ ($x = 0.05$, 0.1, 0.2, 0.3, 0.4, 0.5) after reoxidation at 300 °C for 2 h.

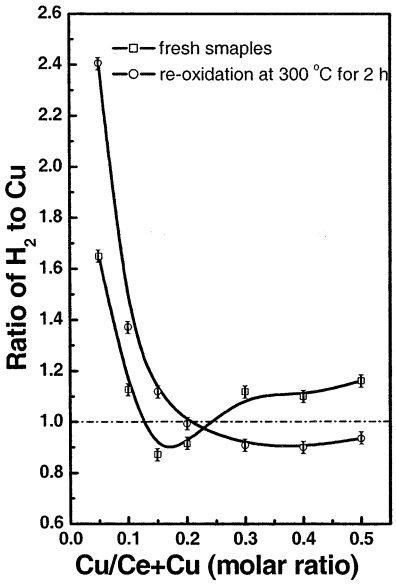

Figure 7. H_2 consumption of $Ce_{1-x}Cu_xO_y$ ($x = 0.05$, 0.1, 0.15, 0.2, 0.3, 0.4, 0.5).

CuO dispersed on the surface of CeO_2 plays an important role. The broad γ peak indicates several Cu^{2+} species coexist; meanwhile, a stepwise reduction mechanism controlled by the kinetic diffusion in bulk CuO is also suggested for higher Cu/(Ce + Cu) molar ratio.

Figure 6 shows the TPR profiles of $Ce_{1-x}Cu_xO_y$ samples reoxidized at 300 °C after the preliminary H_2-TPR measurement. Different from the TPR behaviors of the fresh samples, with the reduction temperature increases, the α peak almost disappeared and the β peak with several shoulders overlapped into a broad peak for the solid solution samples ($x \leq 0.1$), whereas no obvious change was found for the higher Cu/(Ce + Cu) ratio samples. The possible explanations for this phenomenon could be that the transfer between the surface oxygen and the bulk oxygen occurred in the solid solution samples during the reduction−oxidation processes. The reduction of CeO_2 is not limited only to the surface oxygen, but extends to the bulk oxygen as well. So, the β peak is ascribed to the reduction of Cu^{2+} species and the reduction of part of the bulk CeO_2, whereas the redox behavior of the CuO dispersed on the surface of CeO_2 is affected slightly by CeO_2. Thus, the similar TPR profiles are observed and the reduction temperature is slightly higher than that of fresh samples when $x \geq 0.2$.

Figure 7 is a plot of a quantitative analysis of H_2 consumption, where the calculated value was obtained by assuming a complete reduction of the CuO component to Cu, i.e., the ratio of H_2 to Cu is 1.0. For the fresh samples, the $Ce_{0.95}Cu_{0.05}O_y$ showed the highest H_2/Cu ratio, which is about 1.65. A decreased ratio of H_2 to Cu is also obtained for $Ce_{0.9}Cu_{0.1}O_y$, but it is still higher than 1.0. This implies that the surface reduction of Ceria is taking place at low temperatures in the low Cu/(Ce + Cu) ratio samples. However, for the samples consisting of solid solution and CuO clusters ($x = 0.15$, 0.20), the ratio of H_2 to Cu is even lower than 1.0. There are two possibilities for this observation. One possibility is that the CuO cannot be completely reduced to metallic copper because of the kinetic diffusion limitations caused by the smaller BET surface and pore volume. However, this cannot be a major factor because the lack of CuO particles for the Cu content range from 0.15 to 0.3 as mentioned in the XRD results. The other possibility is that Cu^{2+} ions in the $Ce_{1-x}Cu_xO_y$ solid solutions are not completely reduced due to the structure stability, which leads to the decrease of H_2 uptake although partial reduction of CeO_2 is considered. At high Cu/(Ce + Cu) ratio ($x \geq 0.3$), most Cu species exist in the form of CuO that can be reduced completely. Combined with the reduction of surface oxygen of CeO_2, a higher ratio of H_2 to Cu than 1.0 was obtained again. Concerning the samples after reoxidation at 300 °C, the ratio of H_2 to Cu was higher than that of fresh samples when $x \leq 0.2$. In contrast, for the samples $x \geq 0.3$, it was not only lower than that of fresh samples but also lower than 1.0.

On the basis of these observations, the TPR results can be grouped into three parts: $x \leq 0.1$, $0.15 \leq x \leq 0.2$, and $x \geq 0.3$. For the samples with Cu/(Ce + Cu) ratio ≤ 0.1, the redox property is dominated by the formation of $Ce_{1-x}Cu_xO_y$ solid solutions. The incorporation of CuO_x introduces structural defects into the ceria lattice. In this case, cerium ions situated on this axis are six-coordinate, with their near-neighbors being seven-coordinate.[32] This indicates that the ceria sublattice is not strongly perturbed by the defects, which instead cause the formation of a defective oxygen sublattice. The defect is therefore not localized in one single oxygen site but instead extends into additional surrounding oxygen positions. So, many oxygen vacancies are generated with the formation of solid solutions.

The adsorbed oxygen on the $Ce_{1-x}Cu_xO_y$ solid solutions with the oxygen vacancies can be reduced at lower temperature, and the α peak was ascribed to its reduction. So, the H_2 uptake excesses to the calculated value although the Cu^{2+} ions in the solid solutions are not completely reduced. The redox property of the solid solutions is also associated with the formation of oxygen

(32) Trovarelli, A., Ed. *Catalysis by Ceria and Related Materials*Imperial College Press: London, 2002.

vacancies. The electron transfer between Cu, O, and Ce species and oxygen vacancies in the reduction−oxidation processes decreases the redox potentials of CuO and promotes the diffusion of oxygen from the bulk to the surface which enhances the redox action of the Ce^{4+}/Ce^{3+} couples. This accounts for the fact that H_2 uptake of solid solutions increased after the samples were reoxidized at 300 °C.

In the Cu content ranging from 0.15 to 0.2, $Ce_{1-x}Cu_xO_y$ solid solutions and small CuO clusters coexisted as evidenced by XRD results. The small CuO clusters covered part of the oxygen vacancies that led to the decrease of adsorbed oxygen, and the Cu^{2+} ions in the solid solutions were not reduced completely. So the intensity of α peak reduced and the H_2 uptake was less than the calculated value for fresh samples. Although the redox property of the catalysts was also enhanced due to the formation of solid solutions, consequently the highest H_2 uptake was observed for the samples after being reoxidized at 300 °C as compared with the calculated value and fresh samples.

The bulk CuO played an important role in the samples when $x \geq 0.3$. As shown in the XRD results, most Cu^{2+} ions exist in the form of small clusters or bulk CuO, which can be wrapped by CeO_2 during the reduction−oxidation processes. Because of this defect, the CuO and CeO_2 are difficult to reduce and reoxidize due to the kinetic diffusion, resulting in poor reduction capability and redox property.

The redox properties between $Ce_{0.9}Cu_{0.1}O_y$ and $Ce_{0.7}Cu_{0.3}O_y$ are further compared. Figure 8(a) shows the H_2-TPR profiles of $Ce_{0.9}Cu_{0.1}O_y$ treated at different conditions. The numbers in the figure are the ratios of the H_2 consumption at different conditions to that of the fresh sample, representing the reoxidation degree. Compared with the fresh sample, enhanced α, *β* peaks were observed for the sample oxidized at 300 °C for 2 h before the H_2-TPR experiment with the reoxidation degree of 1.17. This suggested that the fresh sample is in an unsaturated state and it is oxidized deeply at 300 °C. After the H_2-TPR experiment, the sample was reoxidized at different temperatures. When it was reoxidized at 100 °C, the α, *β* peaks were restorable partly. With increasing reoxidation temperature up to 200−300 °C, similar H_2-TPR profiles were observed with the α peak disappeared and the *β* peak broadened and shifted to higher reduction temperatures. The reoxidation degree was 1.16 and 1.22, respectively, which is almost consistent with 1.17 in the sample oxidized at 300 °C previous to the H_2-TPR experiment. These results indicated that the energy required to reduce and reoxidize the surface adsorbed oxygen and the Cu^{2+} species is low, and that the oxygen transfers from the surface to the bulk during the reduction and reoxidation processes at higher reoxidation temperatures due to the formation of solid solution with oxygen vacancies. So the α peak disappeared and the increased energy was required for the reduction of bulk oxygen, which explained the broad and shifted *β* peak.

The same experiment process was performed for the $Ce_{0.7}Cu_{0.3}O_y$ sample where most CuO dispersed on the surface of CeO_2. As shown in Figure 8(b), the reoxidation degree was only 0.21 for the sample reoxidized at 100 °C, corresponding to part CuO. The reoxidation degree

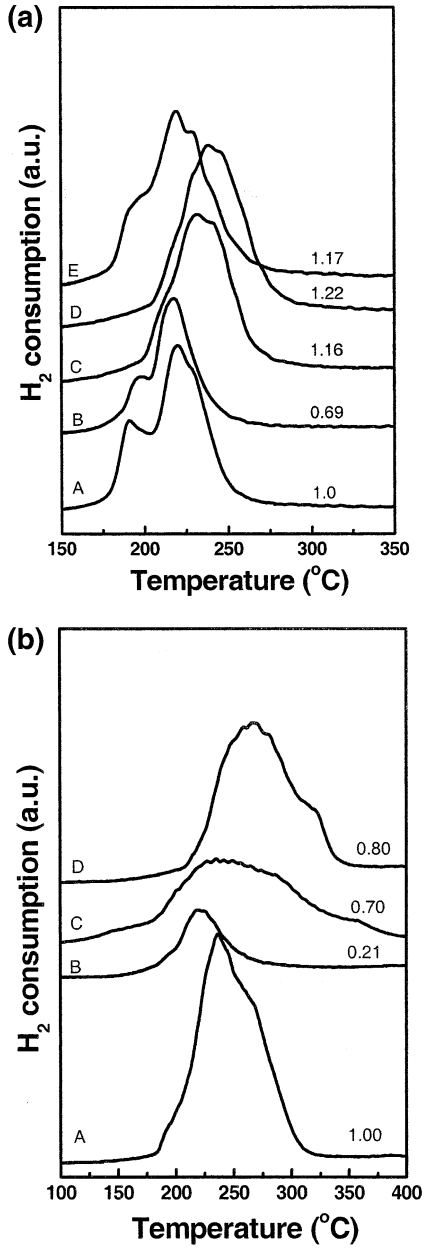

Figure 8. TPR profiles of $Ce_{0.9}Cu_{0.1}O_y$ (a) and $Ce_{0.7}Cu_{0.3}O_y$ (b) treated at different conditions: A, fresh sample; B, reoxidation at 100 °C; C, reoxidation at 200 °C; D, reoxidation at 300 °C; E, oxidation at 300 °C before H_2-TPR experiment.

increased with increasing temperatures, but it was still not higher than 0.80 even at 300 °C, and no evidence for the reduction of CeO_2 was observed. This phenomenon is ascribed to the impediment of oxygen transfer from CuO and CeO_2 in the reduction and reoxidation processes due to the lack of oxygen vacancies. In summary, it is concluded that the reduced redox potentials of the copper and cerium species are available in the $Ce_{0.9}Cu_{0.1}O_y$ solid solution.

The H_2 consumption during the reduction and reoxidation cycles at 300 °C is shown in Figure 9. It can be seen that the $Ce_{0.9}Cu_{0.1}O_y$ shows the stable redox property with an error less than 5%. This result confirmed again that the Cu species in the solid solution are stable, and the structure of solid solution is not damaged even by undergoing several reduction and reoxidation cycles.

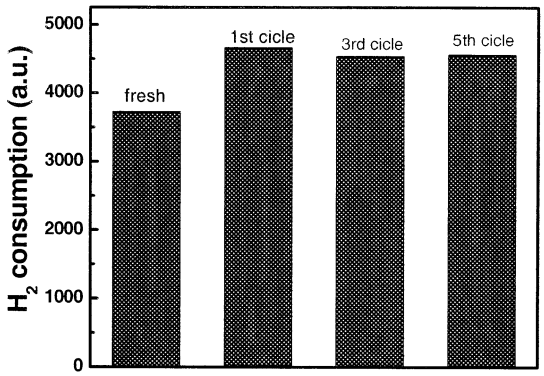

Figure 9. Redox property of $Ce_{0.9}Cu_{0.1}O_y$ undergoing several reduction−oxidation cycles.

Conclusions

The distribution of Cu species in CeO_2 strongly depends on the Cu contents, i.e., the Cu^{2+} ions incorporate into CeO_2 to form solid solutions only at low Cu/(Ce + Cu) ratio ($x \leq 0.1$), and the $Ce_{1-x}Cu_xO_y$ solid solution and small CuO cluster coexist for x in the range from 0.15 to 0.3. The formation of bulk CuO is observed at higher Cu/(Ce + Cu) ratios. The reduction property is also associated with the distribution of Cu^{2+} species. The $Ce_{1-x}Cu_xO_y$ solid solutions ($x \leq 0.1$) have lower reduction temperature and higher H_2 consumption than the high Cu/(Ce + Cu) ratio samples that consist of small CuO clusters and bulk CuO. A quantitative analysis of H_2 consumption suggested that the Cu^{2+} ions incorporated in the CeO_2 lattice are not completely reduced at low temperatures (<500 °C), but the reduction of CeO_2 is enhanced. The comparison of redox property between $Ce_{0.9}Cu_{0.1}O_y$ and $Ce_{0.7}Cu_{0.3}O_y$ at different reoxidation temperatures shows that the mobility of oxygen in surface region and bulk of $Ce_{0.9}Cu_{0.1}O_y$ solid solution becomes very high, indicating that the redox property of $Ce_{0.9}Cu_{0.1}O_y$ solid solution is remarkably improved.

Acknowledgment. We thank Zhonglai Li and Zhibin Lei for significant discussions and constant encouragement, and also Jing Zhang for Raman measurements.

CM0345974